Magnetic Silver Hybrid Nanoparticles for Surface-Enhanced Resonance Raman Spectroscopic Detection and Decontamination of Small Toxic Molecules

Xiao Xia Han,[†] Annette M. Schmidt,[‡] Gernot Marten,[‡] Anna Fischer,[†] Inez M. Weidinger,[†,*] and Peter Hildebrandt[†,*]

[†]Institut für Chemie, Technische Universität Berlin, Strasse des 17. Juni 135, D-10623 Berlin, Germany and [‡]Department Chemie, Universität zu Köln, Luxemburger Str. 116, D-50939 Köln, Germany

ABSTRACT

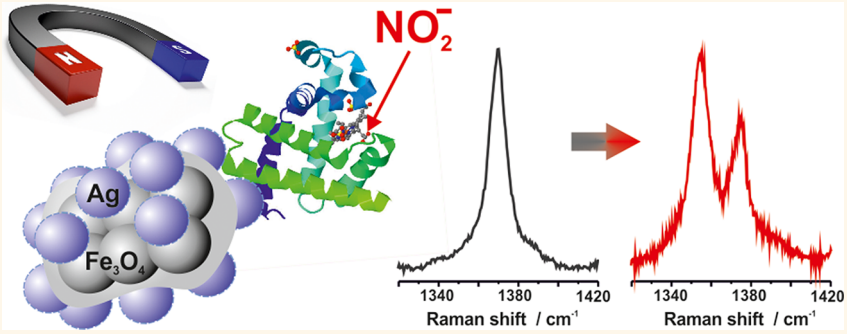

Magnetic hybrid assemblies of Ag and Fe_3O_4 nanoparticles with biocompatibly immobilized myoglobin (Mb) were designed to detect and capture toxic targets (NO_2^-, CN^-, and H_2O_2). Mb was covalently attached to chitosan-coated magnetic silver hybrid nanoparticles (M-Ag-C) *via* glutaraldehyde that serves as a linker for the amine groups of Mb and chitosan. As verified by surface-enhanced resonance Raman (SERR) spectroscopy, this immobilization strategy preserves the native structure of the bound Mb as well as the binding affinity for small molecules. On the basis of characteristic spectral markers, binding of NO_2^-, CN^-, and H_2O_2 could be monitored and quantified, demonstrating the high sensitivity of this approach with detection limits of 1 nM for nitrite, 0.2 μM for cyanide, and 10 nM for H_2O_2. Owing to the magnetic properties, these particles were collected by an external magnet to achieve an efficient decontamination of the solutions as demonstrated by SERR spectroscopy. Thus, the present approach combines the highly sensitive analytical potential of SERR spectroscopy with an easy approach for decontamination of aqueous solutions with potential applications in food and in environmental and medical safety control.

KEYWORDS: magnetic nanoparticles · silver nanoparticles · SERR · toxic small molecule · myoglobin · spectroscopic detection · decontamination

Small toxic molecules present in water and food have a strong impact on human health. Nitrite is a toxic decontaminant in water and agricultural products. It is also commonly used as a preservative, color fixative, and flavoring in meats, fishes, and other food products. Nitrite may cause irreversible oxidation of hemoglobin to methemoglobin and thus abolishes the oxygen transport function.[1] Numerous studies have shown that excessive nitrite uptake contributes to a variety of negative health effects, such as DNA mutation, cancer, and chronic obstructive pulmonary disease.[2,3] Cyanide can tightly bind to ferric hemes such as heme a_3 in cytochrome *c* oxidase and thus blocks intracellular oxygen reduction. H_2O_2, known as a cytotoxic and signaling molecule, is widely utilized as a target in clinical diagnosis, food and pharmaceutical

* Address correspondence to i.weidinger@mailbox.tu-berlin.de, hildebrandt@chem.tu-berlin.de.

Received for review December 20, 2012 and accepted March 14, 2013.

Published online March 15, 2013
10.1021/nn305892j

analysis.[4] So far, many analytical techniques have been developed for such kinds of small toxic molecule detection. A detailed comparison of various approaches (*e.g.*, chemiluminescence, Griess and fluorescence-based techniques) for nitrate and nitrite detection was reviewed by Moorcroft *et al.*[5] Electrometric[6] and chromatographic[7] methods were used for cyanide detection, which required a relatively long procedure, and a gold NP-based fluorescent sensor was found to be a more rapid and cost-effective way.[8] Due to their redox capabilities, heme proteins have been utilized in bioelectrochemical sensors for H_2O_2.[9] Recently, carbon nanotubes and graphene have received increasing interest in their application in H_2O_2 sensing.[10,11] Among these techniques, however, none of them display simultaneously the desired high sensitivity and easy operation as well as the capability of decontamination.

In recent years, analytical techniques based on surface-enhanced Raman (SER) scattering have attracted increasing interest in biochemistry, biomedicine, food and environmental safety control.[12−16] The sensitivity of this technique is particularly strong when the Raman excitation line is in resonance with both the surface plasmons of the nanostructured metal (Ag or Au) and an electronic transition of a chromophore of the target molecule, such that the SER and resonance Raman (RR) effect combine (surface-enhanced resonance Raman, SERR).[12] Heme proteins are particularly appropriate for SERR spectroscopy (*e.g.* cytochrome *c*) since the heme cofactor gives rise to very strong signals upon excitation in the violet region.[17,18]

Applying SER or SERR spectroscopy to biomolecules requires an appropriate biocompatible coating of the metal surface to avoid denaturation and thus the loss of the native structural and functional properties.[19] Possible coatings that fulfill these requirements include self-assembled monolayers of amphiphiles,[17] (bio)polymers, or oxides as demonstrated for shell-isolated nanoparticles (NPs) that are Au or Ag nanoparticles coated by Al_2O_3, SiO_2, or chitosan.[19−21]

Due to their inherent magnetic properties, Fe_3O_4 NPs of various sizes have gained increasing popularity in biology and medicine as they may be employed in protein purification, bioseparation, medical imaging, and drug delivery.[22−27] In view of this wide range of applications, it is of particular interest to design hybrid NPs that combine these magnetic properties with plasmonic activity[28] to allow for simultaneous magnetic control of the NPs and SER/SERR spectroscopic monitoring of adsorbates. First results in this respect have been recently reported,[29,30] although those NPs lack an appropriate biocompatible coating and thus may limit the general applicability for binding biomolecules.

In this work, we developed magneto-plasmonic hybrid devices to explore the potential for detecting and decontaminating small toxic molecules. The devices consist of Fe_3O_4 NP cores in a silica matrix and a shell of Ag NPs coated by chitosan. The size of the Ag NPs is chosen to tune the plasmonic frequency to the electronic transition of the heme cofactor of the biosensor myoglobin (Mb) for optimum SERR enhancement. Mb was covalently attached to chitosan using glutaraldehyde as a linker. SERR spectroscopy was then employed to monitor binding of small toxic molecular species (NO_2^-, CN^-, and H_2O_2) by the immobilized Mb. The present approach not only fulfills the requirements of a rapid and effective sensor suitable for food and environmental safety control but also displays a decontamination ability, lacking in the previous analytical techniques.

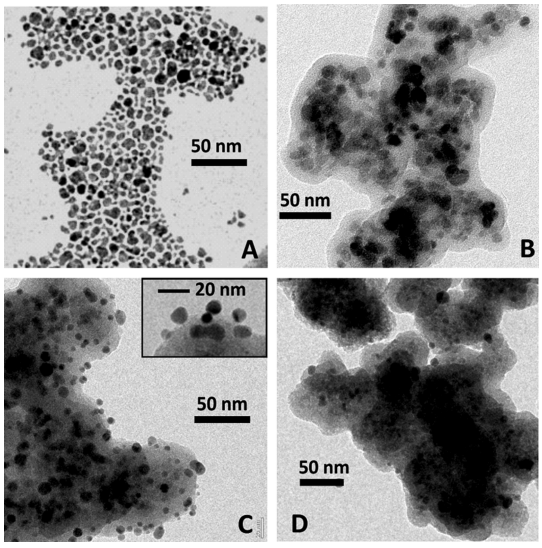

Figure 1. TEM images of (A) Fe_3O_4, (B) Fe_3O_4−SiO_2, (C) Fe_3O_4−SiO_2−Ag_{seed}, and (D) Fe_3O_4−SiO_2−Ag_{seed}−Ag−chitosan; the inset in C is a magnified image selected from a region of Fe_3O_4−SiO_2−Ag_{seed}.

RESULTS AND DISCUSSION

Preparation of Magnetic Ag Nanoparticles. Magnetic (Fe_3O_4) NPs were obtained by alkaline precipitation of ferric and ferrous iron salts from aqueous acidic solution[31] and electrostatically stabilized in water by treatment with citric acid.[32] As observed in transmission electron microscopy (TEM), they possess an average diameter of 10 nm (Figure 1A).

Silica coating resulted in the formation of bigger nanocomposites consisting of small Fe_3O_4 NP aggregates surrounded by a silica layer with an average thickness of 10 nm (Figure 1B). The silica layer was subsequently functionalized with 3-aminopropyltrimethoxysilane (APTMS)[33,34] to allow for electrostatic binding of Ag seeds (small Ag NPs) with negatively charged surface.[35] Addition of Ag seeds resulted in attachment of small Ag NPs with an average diameter of 12 nm[36] to the silica surface (Figure 1C). The Ag NPs were grown subsequently mediated by the Ag seeds on the silica-coated Fe_3O_4 NPs. Ag NP aggregates in Figure 1D arose from the growth of Ag NPs (Figure 1C),

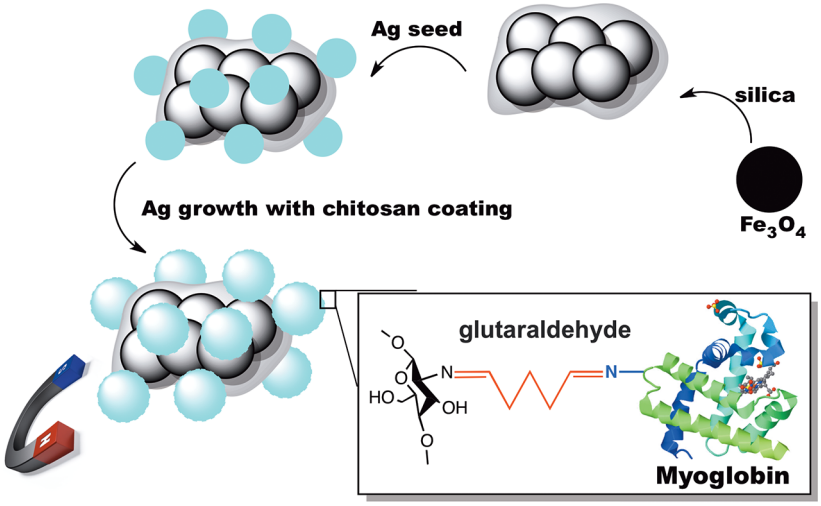

Figure 2. Scheme of coating and functionalizing magnetic NPs with silica, Ag, chitosan, and Mb.

which decreased the distance between Ag NPs and thus increased the Ag aggregation. During the growth process, simultaneous coating with chitosan[20] resulted in the formation of a chitosan layer (Figure 1D). In a last step, covalent binding of Mb was achieved by using glutaraldehyde as cross-linkers for Schiff base.

$$\text{chitosan} - NH_2 + OHC(CH_2)_3CHO + H_2N - \text{Mb} \rightarrow \text{chitosan} - N{=}C(CH_2)_3C{=}N - \text{Mb} \quad (1)$$

For SERR measurements, a magnet was placed at the bottom of the solution, causing aggregation of the Fe_3O_4–Ag nanocomposites on top of the magnet. The individual steps are illustrated in Figure 2.

Optical Properties of Magnetic Nanoparticles Coated with Silica, Ag, and Chitosan. The growth conditions of the Ag NPs were optimized with respect to their plasmonic properties and their ability to enhance the SERR signal of surface-bound Mb. In the UV–vis spectra of Fe_3O_4 NPs without and with SiO_2 coating (Figure 3, traces B and C), no absorption due to a plasmonic resonance can be seen. The spectra of the Ag seeds show a characteristic surface plasmon resonance at 388 nm (Figure 3, trace A) as expected for particles of this size.[37,38] After coating Fe_3O_4–SiO_2 with Ag seeds, the plasmon resonance of Ag was red-shifted by 11 to 399 nm (Figure 3, trace D), indicating that these small Ag NPs are attached to the silica surface. The plasmon resonance of Ag is further red-shifted to *ca.* 440 nm and broadened with the growth of Ag NPs (Figure 3, trace E). This absorption band overlaps with the Soret bands of the various states of Mb (408–435 nm) such that it is possible to select an excitation line that coincides with both the plasmonic resonance and the electronic transition of the heme chromophore, as a prerequisite for an optimum surface enhancement of the RR spectrum (*vide infra*, Supporting Information, Figure S1).

Biocompatibility of the M-Ag-C. A strong Raman signal enhancement is expected for close junctions of adjacent Ag NPs.[39–41] Therefore, high-quality SERR spectra of Mb could be obtained after accumulation of the Mb-loaded M-Ag-C NPs on the magnet. The spectra are shown in Figure 4 together with the corresponding RR and SERR spectrum of Mb in solution and adsorbed on bare Ag NPs synthesized by aqueous reduction of Ag nitrate (10^{-3} M, 200 mL) with trisodium citrate (1%, 4 mL).[42] As reported previously, we also found that binding to bare Ag NPs caused a conformational change of the heme protein (Figure 4). For a six-coordinated high-spin (6cHS) configuration of the heme, the ν_3 band appears at 1479 cm^{-1} in the RR spectrum of Mb, but the band is shifted to 1489 cm^{-1} on bare Ag surfaces. Another useful marker band for the 6cHS state, the ν_2 mode at 1562 cm^{-1}, is broadened and shifted to 1565 cm^{-1} (Supporting Information, Table S1). Both of these shifts are attributed to a non-native 5cHS state of the heme upon the interactions with bare Ag.[43] In contrast, the SERR spectrum of Mb bound to the M-Ag-C NPs is quite similar to the RR spectrum of native Mb in solution, indicating that the biocompatibility of the particles has been remarkably improved without lowering the SERR intensity. The surface enhancement provided by M-Ag-C NPs is determined to be 16, but the measured intensity is further increased by a factor of *ca.* 4 upon magnetic collection of the particles (Supporting Information, Figure S3). The chitosan coating is also important for M-Ag NPs in applications for decontaminating toxic compounds because the biocompatible surface is likely to avoid possible interactions of the target molecules directly with the Ag surface.

Nitrite Binding to Mb. Nitrite binding to Mb(Fe^{3+}) is supposed to produce Mb(Fe^{3+}–NO_2^-), and such kind of binding is reversible (eq 2).[44]

$$\text{Mb}(Fe^{3+}) + NO_2^- \rightleftharpoons \text{Mb}(Fe^{3+}{-}NO_2^-) \quad (2)$$

After addition of sodium dithionite (SD), the ferric Mb is reduced to the ferrous state. In addition, excess

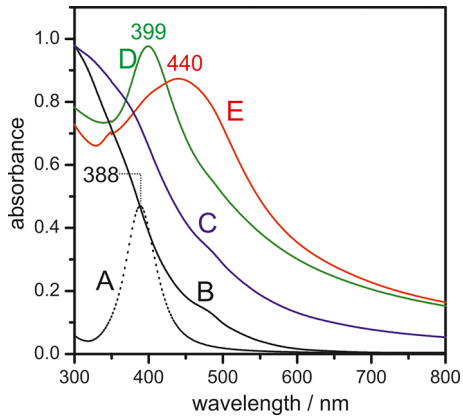

Figure 3. UV−vis spectra of Ag seed (A, dotted line), Fe_3O_4 NPs (B, black), Fe_3O_4 NPs coated with silica (C, blue), Ag (D, green), and chitosan (E, red).

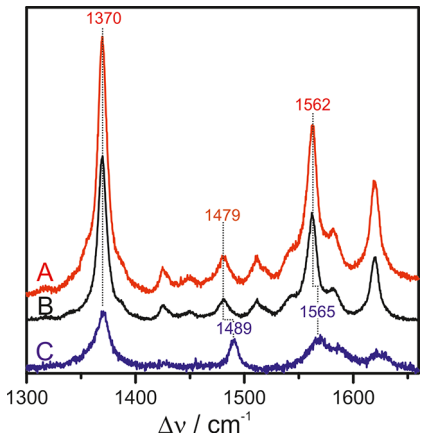

Figure 4. RR spectrum of Mb (1 mg/mL) in solution (B, black) and SERR spectra of Mb (0.1 mg/mL) on bare Ag NPs (C, blue) and M-Ag-C NPs (A, red). Experimental conditions are given in the text.

SD consumes oxygen in solution, and thus the ferrous Mb largely exists in the deoxy form (eq 3).

$$\mathrm{Mb(Fe^{3+})} + \mathrm{SD} \rightarrow \mathrm{deoxyMb(Fe^{2+})} \quad (3)$$

The reaction between nitrite and deoxygenated ferrous Mb yields NO and the ferric state (eq 4), with NO subsequently being captured by the remaining non-oxidized deoxyMb to afford nitrosyl-Mb [Mb(Fe^{2+}-NO)] (eq 5).[45]

$$\mathrm{deoxyMb(Fe^{2+})} + \mathrm{NO_2^-} \rightarrow \mathrm{Mb(Fe^{3+})} + \mathrm{NO} \quad (4)$$

$$\mathrm{deoxyMb(Fe^{2+})} + \mathrm{NO} \rightarrow \mathrm{Mb(Fe^{2+} - NO)} \quad (5)$$

NO has a high affinity to deoxyMb such that binding is essentially irreversible. The formation of these complexes of Mb in solution can be monitored by the respective UV−vis spectra (Figure 5). Note that the doublet at 548 and 580 nm confirms the formation of Mb(Fe^{2+}−NO) in the mixture of Mb, nitrite, and SD.[46]

The reactions in eqs 2−5 were also probed by RR spectroscopy (Figure 6). The RR spectrum of Mb(Fe^{3+}) shows the ν_4 band at 1370 cm^{-1} characteristic of a 6cHS state. After reduction by SD, the band is shifted to 1354 cm^{-1}, corresponding to the 5cHS state of the deoxygenated Mb(Fe^{2+}). After nitrite binding to Mb(Fe^{3+}), the ν_4 band undergoes a slight upshift with a shoulder on the high-frequency side. Upon addition of SD, two separated bands at 1354 and 1375 cm^{-1} can be observed that originate from the deoxygenated Mb(Fe^{2+}) and Mb(Fe^{2+}−NO) form,[47,48] respectively. The relative intensity ratio of the two bands is sensitive to the nitrite concentration, indicating the possibility of nitrite detection using RR spectroscopy.

Quantitative Detection and Decontamination. The M-Ag-C NPs were dispersed in nitrite-containing solution to capture nitrite. The target molecules, bound as NO_2^- to the immobilized Mb, were concentrated by "magnetic separation" *via* an external magnet. As shown in Figure 7A, the intensity ratio of the band at 1375 cm^{-1} compared to that at 1354 cm^{-1} increased remarkably with the increasing nitrite concentration. The limit of detection (LOD) for sodium nitrite of this method is thus estimated to be 1.4 nM (Figure 7B).

In the concentration range between 10^{-9} and 10^{-6} mol/L, a fit to the data shown in Figure 7B gave the following calibration curve (eq 6)

$$\log[\mathrm{NO_2^-}] = 21.4 \cdot \frac{I_{1375}}{I_{1354}} - 15.2 \quad (6)$$

which allows quantitative determination of an unknown nitrite concentration from the SERR spectrum.

The separation of the magnetic nanoparticles by the external magnet not only allows for a sensitive detection of nitrite but also represents a convenient procedure for decontaminating the toxic targets. As shown in Figure 7C, the relative SERR intensity of the band at 1375 cm^{-1} significantly decreased after such decontamination, indicating that most of the nitrite (>90%) was removed. Moreover, these kinds of magnetic nanoparticles are nontoxic and, thus, may be used to decontaminate nitrite in water, food, or agricultural products.

Cyanide and H_2O_2 Bindings to Mb. Besides nitrite, also cyanide and H_2O_2 can bind to the heme group in Mb. The underlying processes (eqs 7 and 8) are reflected by the UV−vis spectra (Figure 8).[49,50]

$$\mathrm{Mb(Fe^{3+})} + \mathrm{CN^-} \rightarrow \mathrm{Mb(Fe^{3+}-CN^-)} \quad (7)$$

$$\mathrm{Mb(Fe^{3+})} + \mathrm{H_2O_2} \rightarrow \mathrm{Mb(Fe^{4+}{=}O)} + \mathrm{H_2O} \quad (8)$$

The SERR spectra of Mb on M-Ag-C NPs are sensitive to the binding of cyanide. As shown in Figure 9, the ν_4 band at 1370 cm^{-1} of met-Mb(Fe^{3+}) is gradually shifted to 1373 cm^{-1} with increasing cyanide concentrations. Cyanide binding is also reflected by the decrease of the ν_2 band intensity at 1562 cm^{-1} (6cHS state of Mb(Fe^{3+})) and the shift of the ν_3 band

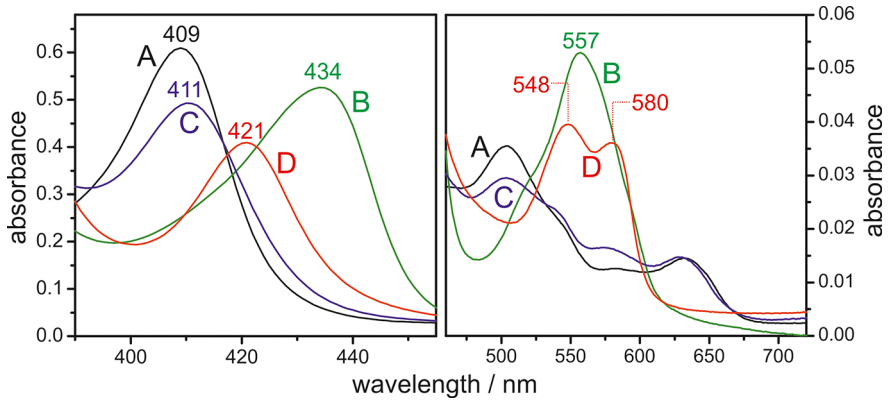

Figure 5. UV−vis spectra of Mb (A, black), Mb with SD (B, green), Mb with sodium nitrite (C, blue), and Mb with nitrite and SD in PBS buffer at pH 7 (D, red). Mb (1 mg/mL), SD (10 mg/mL), and nitrite (10 mg/mL) were mixed with volume ratios of 1:1 or 1:1:1 before dilution for UV−vis measurements. The left and right panels show the Soret and Q-band region, respectively.

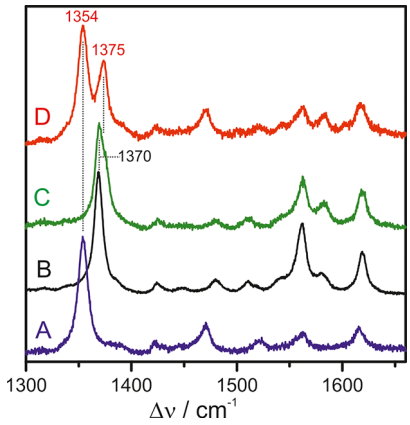

Figure 6. RR spectra of Mb (B, black), Mb with SD (A, blue), Mb with nitrite (C, green), Mb with nitrite and SD in PBS buffer at pH 7 (D, red). Mb (1 mg/mL), SD (10 mg/mL), and nitrite (1 mg/mL) were mixed with the volume ratios of 1:1 or 1:1:1 prior to the RR measurements.

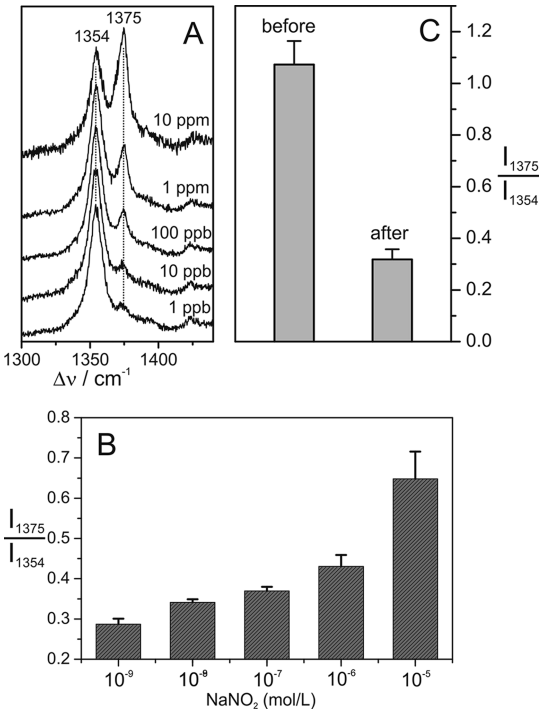

Figure 7. (A) SERR spectra displaying the Mb(Fe^{2+}) (1354 cm^{-1}) and Mb(Fe^{2+}−NO) (1375 cm^{-1}) mixtures as a function of the $NaNO_2$ concentration; (B) SERR intensity ratio of the bands at 1375 and 1354 cm^{-1} *versus* the $NaNO_2$ concentration; (C) SERR intensity ratio of the bands at 1375 and 1354 cm^{-1} at 10 ppm $NaNO_2$ before and after twice decontamination with the Mb-coated M-Ag-C NPs. Each error bar represents a standard deviation from three batches.

from 1479 to 1507 cm^{-1}. All of these spectral changes indicate the formation of 6cLS state of the ferric 6cLS heme−CN complex at the expense of the 6cHS configuration of met-Mb. The corresponding LOD for sodium cyanide is estimated to be *ca.* 0.2 μM.

For H_2O_2 binding to immobilized met-Mb, the ν_4 band is shifted to 1377 cm^{-1} and its intensity increases with increasing H_2O_2 concentrations (Figure 10), which may be attributed to the formation of the Mb(Fe^{4+}=O) complex.[49] Further spectral changes are also noted in the region of the ν_2 and the ν_3 bands. The quantitative analysis of these spectra indicates a LOD for H_2O_2 of *ca.* 10 nM. As in the case of nitrite, the Mb-functionalized M-Ag-C NPs were also found to be capable of removing most of the cyanide and H_2O_2 from the solution (data not shown).

Toxic Target Quantification and Potential Applications. Binding of each of the three toxic targets can be quantified by using the Mb-functionalized M-Ag-C NPs according to their specific ν_4 bands at 1375 cm^{-1} for nitrite, 1373 cm^{-1} for cyanide, and 1377 cm^{-1} for H_2O_2. The LOD was determined by the lowest concentration of the toxic molecules that can be detected by SERR spectroscopy, according to these specific Raman bands. The LOD varies from one toxic molecule to another, which is partly related to different binding constants,[44,51,52] but it should also depend on the characteristics of specific ν_4 bands. At very low target molecule concentration, the bands at 1377 and 1373 cm^{-1} overlapped with that at 1370 cm^{-1}, which would obscure these ν_4 bands. In contrast, the band at 1375 cm^{-1} is clearer even at very low nitrite

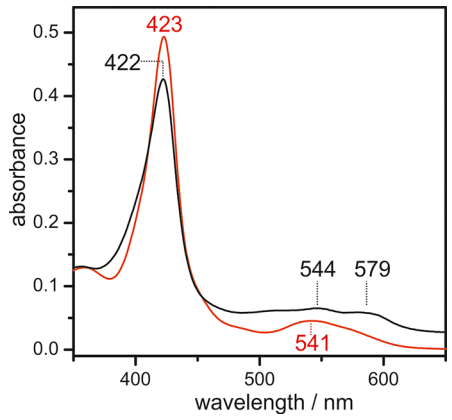

Figure 8. UV−vis spectra of Mb after interactions with sodium cyanide (red) and H_2O_2 (black). Mb (1 mg/mL), sodium cyanide (10 mg/mL), and H_2O_2 (0.1 M) were mixed with the volume ratio of 1:1 before dilution for UV−vis measurements.

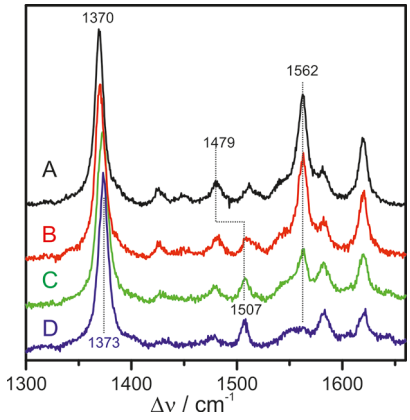

Figure 9. SERR spectra of Mb on M-Ag-C NPs in the absence (met-Mb, A, black) and in the presence of 0.2 μM (B, red), 2 μM (C, green), and 20 μM (D, blue) NaCN in solution.

concentration because there was no band at 1370 cm^{-1} due to the reduction of SD in that case.

In a complex system containing all three toxic targets (Figure S2A), nitrite ions can be easily distinguished in a quantitative manner *via* reduction by SD because, in the presence of excessive SD, only nitrite (*i.e.*, NO) binds to the heme [Mb(Fe^{2+}−NO)], whereas Mb(Fe^{3+}−CN) and Mb(Fe^{4+}=O) are reduced to deoxy-Mb. Distinguishing cyanide ions and H_2O_2 would need a more detailed analysis of their composite ν_4 bands. As shown in Figure S2B, in a mixture of CN^- and H_2O_2, a composite band was observed, consisting of two specific ν_4 bands from Mb(Fe^{3+}−CN^-) and Mb(Fe^{4+}=O).

The maximum contaminant level (MCL) in drinking water set by the U.S. Environmental Protection Agency (EPA) is 1 ppm (20 μM) for nitrite and 200 ppb (7.7 μM)

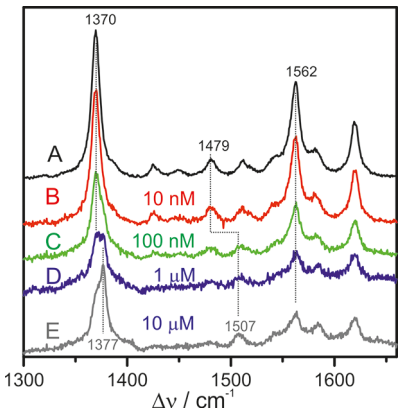

Figure 10. SERR spectra of Mb on M-Ag-C NPs at different H_2O_2 concentrations.

for cyanide.[53] The LODs of the present approach is 1 nM and 0.2 μM for nitrite and cyanide, respectively, and are thus in both cases distinctly lower than the respective MCL. For H_2O_2, the present method is comparable to the lowest LOD among a variety of H_2O_2 sensors reported in recent years.[9] Besides these toxic targets (NO_2^-/NO, CN^-, and H_2O_2) reported in our study, other toxic molecules/ions, such as CO, F^-, or H_2S/HS^-, also can bind to Mb, resulting in variation of the ν_4 mode of Mb.[54−56] Therefore, the Mb-functionalized M-Ag-C NPs should be applicable to toxic target detection and, as a unique property of this approach, for decontamination, offering novel applications in food, environmental, and clinical analysis and detoxification.

CONCLUSIONS

We designed and synthesized M-Ag-C NPs that allow for immobilization of Mb under preservation of its function to bind small toxic molecules. The hybrid NPs exhibit tailored plasmonic properties for SERR spectroscopic detection of the binding of target molecules by the heme group of Mb. Thus, this spectroscopic technique offers the possibility to quantify the concentration of nitrite, cyanide, and hydrogen peroxide in solution with detection limits that are lower than the respective MCL values. Due to the magnetic properties, dispersed M-Ag-C NPs with bound toxic targets can be easily collected by an external magnet, representing a convenient way for decontamination. Furthermore, the way of covalent Mb binding to the particle surface as used in this work is of general applicability and thus could be as well employed for immobilizing other protein (*e.g.*, enzymes and antibodies), thereby opening a variety of applications for M-Ag NPs in bioanalytics and biosensoring.

EXPERIMENTAL SECTION

Preparation of Magnetic Nanoparticles. Magnetite (Fe_3O_4) nanoparticles were prepared according to the procedure of Massart and Cabuil[31] by alkaline precipitation of $FeCl_2$ and $FeCl_3$ solution under inert conditions. After careful washing cycles with deionized water, the particles were redispersed in 2 M nitric acid and

stirred for 5 min. The particles were washed with nitric acid and water and dispersed in 0.01 M cirtric acid and stirred for 5 min; after separation of the supernatant, the particles were dispersed in tetramethylammonium hydroxide aqueous solution.[32]

Coating Magnetic Nanoparticles with Silica, Ag, and Chitosan. *Fe_3O_4—SiO_2.* Fe_3O_4 (0.5 mL) (2.26 wt % in H_2O) was dispersed in aqueous trisodium citrate solution (0.3 M) at 80 °C to improve the dispersion stability of the magnetic NPs.[57] After 1 h, the Fe_3O_4 NPs were collected by a magnet, followed by washing with ethanol and deionized water.

The trisodium citrate-pretreated Fe_3O_4 NPs were redispersed with a mixture of ethanol (120 mL), H_2O (40 mL), and ammonia solution (3 mL, 28 wt %) under mechanical stirring for 15 min, followed by dropwise addition of tetraethyl orthosilicate (TEOS, 1 mL) within 2 min.[35] The entire mixture was mechanically stirred for 5 h, and then the particles were separated and collected with a magnet, followed by washing with ethanol and deionized water.

Ag Seed. $AgNO_3$ (2 mL) (1% w/v) and 4 mL of trisodium citrate solution (0.038 M) were added in a flask with 200 mL of distilled water in an ice bath under stirring. Then, 0.6 mL of $NaBH_4$ (0.01% w/v) was added dropwise, and the mixture was kept in an ice bath under stirring for 2 h and then stored in the refrigerator.[36]

Fe_3O_4—SiO_2—Ag_{seed}. The magnetic Fe_3O_4—SiO_2 NPs were dispersed in 1% APTMS aqueous solution and stirred for 4 h.[58] The APTMS-functionalized magnetic Fe_3O_4—SiO_2 NPs were magnetically separated from the mixture solution and then washed with ethanol and deionized water.

Twenty milliliters of the Ag seed solution was mixed with 25 mL of aqueous dispersion of APTMS—Fe_3O_4—SiO_2 particles by quick ultrasonication in a water bath.[35] The mixture was subjected to mechanical stirring for 2 h, and the Fe_3O_4—SiO_2—Ag_{seed} particles were separated and washed with deionized water.

Fe_3O_4—SiO_2—Ag—Chitosan (M-Ag-C). Aqueous solutions of trisodium citrate (9.8 mM, 100 mL), ascorbic acid (0.1 M, 25 mL), chitosan (4 mg/mL, 5 mL in 1% acetic acid), and Fe_3O_4—SiO_2—Ag_{seed} were combined at 35 °C. To this mixture was added $AgNO_3$ (0.01 M, 500 μL) dropwise immediately under continuous stirring.[20] The growth of silver NPs ended within 30 min under stirring. The M-Ag-C particles were then separated and washed with deionized water.

Mb Immobilization. The M-Ag-C particles were redispersed in 2.5% glutaraldehyde with a small amount of ethanol and stirred for 2 h,[59] followed by separation and washed with ethanol and deionized water. Then the particles were redispersed in 20 mL of PBS buffer (pH = 7) and mixed (1:1, v/v) with 5 mL of 1 mg/mL Mb (from equine skeletal muscle, M0630 sigma) solution (PBS buffer, pH = 7) with 1 h incubation. Finally, the Mb-attached M-Ag-C NPs were separated, washed, and redispersed with 5 mL of PBS buffer (pH = 7) and then stored in a 4 °C refrigerator.

UV—Vis Spectroscopic and TEM Characterization. UV—vis spectra were collected by a spectrophotometer of CARY 4000 (Agilent Technologies), and TEM measurements were performed on a FEI Tecnai G^2 20 S-TWIN, operated at 200 kV.

Raman Measurements. The Mb-attached M-Ag-C NPs were dispersed in the solution of the toxic target and separated by a magnet within 5 min. SERR spectra were obtained using a confocal Raman spectrometer (LabRam HR-800, Jobin Yvon) with 413 nm excitation (Coherent Innova 300 c Krypton cw laser). The laser beam with a power of 1.0 mW on the samples was focused by a Nikon 20× objective with a 20 mm working distance. For the nitrite system, all samples were collected on a magnet with 20 μL of 10 mg/mL SD. All of the samples were mechanically rotated during Raman measurements to avoid laser-induced protein denaturation. All measurements were taken with 10 s accumulation and 5 scan cycles.

Conflict of Interest: The authors declare no competing financial interest.

Acknowledgment. X.X.H. acknowledges a fellowship from the Alexander von Humboldt Foundation. The work was supported by the Fonds der Chemischen Industrie (I.M.W.), the DFG (Cluster of Excellence UniCat, P.H., I.M.W.), and the Senate of Berlin ("Nachhaltige Chemie") (P.H.).

Supporting Information Available: UV—vis absorption and SERR spectra of Mb adducts on M-Ag-C NPs, a table including the most important SERR/RR bands of Mb, and details of the enhancement factor determination. This material is available free of charge *via* the Internet at http://pubs.acs.org.

REFERENCES AND NOTES

1. Yue, R.; Lu, Q.; Zhou, Y. A Novel Nitrite Biosensor Based on Single-Layer Graphene Nanoplatelet—Protein Composite Film. *Biosens. Bioelectron.* **2011**, *26*, 4436–4441.
2. Jiang, R.; Paik, D. C.; Hankinson, J. L.; Barr, R. G. Cured Meat Consumption, Lung Function, and Chronic Obstructive Pulmonary Disease among United States Adults. *Am. J. Respir. Crit .Care Med.* **2007**, *175*, 798–804.
3. Larsson, S. C.; Orsini, N.; Wolk, A. Processed Meat Consumption and Stomach Cancer Risk: A Meta-Analysis. *J. Natl. Cancer Inst.* **2006**, *98*, 1078–1087.
4. Yuan, C. J.; Wang, Y. C.; Reiko, O. Improving the Detection of Hydrogen Peroxide of Screen-Printed Carbon Paste Electrodes by Modifying with Nonionic Surfactants. *Anal. Chim. Acta* **2009**, *653*, 71–76.
5. Moorcroft, M. J.; Davis, J.; Compton, R. G. Detection and Determination of Nitrate and Nitrite: A Review. *Talanta* **2001**, *54*, 785–803.
6. Timofeyenko, Y. G.; Rosentreter, J. J.; Mayo, S. Piezoelectric Quartz Crystal Microbalance Sensor for Trace Aqueous Cyanide Ion Determination. *Anal. Chem.* **2007**, *79*, 251–255.
7. Ishii, A.; Seno, H.; Watanabe-Suzuki, K.; Suzuki, O.; Kumazawa, T. Determination of Cyanide in Whole Blood by Capillary Gas Chromatography with Cryogenic Oven Trapping. *Anal. Chem.* **1998**, *70*, 4873–4876.
8. Liu, Y.; Ai, K.; Cheng, X.; Huo, L.; Lu, L. Gold-Nanocluster-Based Fluorescent Sensors for Highly Sensitive and Selective Detection of Cyanide in Water. *Adv. Funct. Mater.* **2010**, *20*, 951–956.
9. Chen, W.; Cai, S.; Ren, Q. Q.; Wen, W.; Zhao, Y. D. Recent Advances in Electrochemical Sensing for Hydrogen Peroxide: A Review. *Analyst* **2012**, *137*, 49–58.
10. Tang, N.; Zheng, J.; Sheng, Q.; Zhang, H.; Liu, R. A Novel H_2O_2 Sensor Based on the Enzymatically Induced Deposition of Polyaniline at a Horseradish Peroxide/Aligned Single-Wall Carbon Nanotubes Modified Au Electrode. *Analyst* **2011**, *136*, 781–786.
11. Shao, Y. Y.; Wang, J.; Wu, H.; Liu, J.; Aksay, I. A.; Lin, Y. H. Graphene Based Electrochemical Sensors and Biosensors: A Review. *Electroanalysis* **2010**, *22*, 1027–1036.
12. Kneipp, K.; Moskovits, M.; Kneipp, H. *Surface-Enhanced Raman Scattering: Physics and Applications*; Springer: Berlin, Germany, 2006.
13. Schlücker, S. *Surface Enhanced Raman Spectroscopy: Analytical, Biophysical and Life Science Applications*; Wiley-VCH: Weinheim, Germany, 2010.
14. Murgida, D. H.; Hildebrandt, P. Disentangling Interfacial Redox Processes of Proteins by SERR Spectroscopy. *Chem. Soc. Rev.* **2008**, *37*, 937–945.
15. Han, X. X.; Ozaki, Y.; Zhao, B. Label-Free Detection in Biological Applications of Surface-Enhanced Raman Scattering. *TrAC, Trends Anal. Chem.* **2012**, *38*, 67–78.
16. Hodges, M. D.; Kelly, J. G.; Bentley, A. J.; Fogarty, S.; Patel, I. I.; Martin, F. L.; Fullwood, N. J. Combining Immunolabeling and Surface-Enhanced Raman Spectroscopy on Cell Membranes. *ACS Nano* **2011**, *5*, 9535–9541.
17. Murgida, D. H.; Hildebrandt, P. Electron-Transfer Processes of Cytochrome *c* at Interfaces. New Insights by Surface-Enhanced Resonance Raman Spectroscopy. *Acc. Chem. Res.* **2004**, *37*, 854–861.
18. Feng, J. J.; Gernert, U.; Sezer, M.; Kuhlmann, U.; Murgida, D. H.; David, C.; Richter, M.; Knorr, A.; Hildebrandt, P.; Weidinger, I. M. Novel Au—Ag Hybrid Device for Electrochemical SE(R)R Spectroscopy in a Wide Potential and Spectral Range. *Nano Lett.* **2009**, *9*, 298–303.
19. Li, J. F.; Huang, Y. F.; Ding, Y.; Yang, Z. L.; Li, S. B.; Zhou, X. S.; Fan, F. R.; Zhang, W.; Zhou, Z. Y.; Wu, Y.; *et al.* Shell-Isolated

Nanoparticle-Enhanced Raman Spectroscopy. *Nature* **2010**, *464*, 392–395.
20. Potara, M.; Gabudean, A.-M.; Astilean, S. Solution-Phase, Dual LSPR-SERS Plasmonic Sensors of High Sensitivity and Stability Based on Chitosan-Coated Anisotropic Silver Nanoparticles. *J. Mater. Chem.* **2011**, *21*, 3625–3633.
21. Sivanesan, A.; Kozuch, J.; Ly, H. K.; Kalaivani, G.; Fischer, A.; Weidinger, I. M. Tailored Silica Coated Ag Nanoparticles for Non-invasive Surface Enhanced Raman Spectroscopy of Biomolecular Targets. *RSC Adv.* **2012**, *2*, 805–808.
22. Gao, J.; Gu, H.; Xu, B. Multifunctional Magnetic Nanoparticles: Design, Synthesis, and Biomedical Applications. *Acc. Chem. Res.* **2009**, *42*, 1097–1107.
23. Liu, J.; Qiao, S. Z.; Hu, Q. H.; Lu, G. Q. Magnetic Nanocomposites with Mesoporous Structures: Synthesis and Applications. *Small* **2011**, *7*, 425–443.
24. Latham, A. H.; Williams, M. E. Controlling Transport and Chemical Functionality of Magnetic Nanoparticles. *Acc. Chem. Res.* **2008**, *41*, 411–420.
25. Gelbrich, T.; Reinartz, M.; Schmidt, A. M. Active Ester Functional Single Core Magnetic Nanostructures as a Versatile Immobilization Matrix for Effective Bioseparation and Catalysis. *Biomacromolecules* **2010**, *11*, 635–642.
26. Xiao, L.; Li, J.; Brougham, D. F.; Fox, E. K.; Feliu, N.; Bushmelev, A.; Schmidt, A.; Mertens, N.; Kiessling, F.; Valldor, M. Water-Soluble Superparamagnetic Magnetite Nanoparticles with Biocompatible Coating for Enhanced Magnetic Resonance Imaging. *ACS Nano* **2011**, *5*, 6315–6324.
27. Marten, G. U.; Gelbrich, T.; Ritter, H.; Schmidt, A. M. A Magnetoresponsive Drug Delivery System *via* β-Cyclodextrin Functionalized Magnetic Polymer Brushes. *IEEE Trans. Magn.* **2013**, *49*, 364–372.
28. Levin, C. S.; Hofmann, C.; Ali, T. A.; Kelly, A. T.; Morosan, E.; Nordlander, P.; Whitmire, K. H.; Halas, N. J. Magnetic-Plasmonic Core−Shell Nanoparticles. *ACS Nano* **2009**, *3*, 1379–1388.
29. Chen, S.; Yuan, Y.; Yao, J.; Han, S.; Gu, R. Magnetic Separation and Immunoassay of Multi-antigen Based on Surface Enhanced Raman Spectroscopy. *Chem. Commun.* **2011**, *47*, 4225–4227.
30. Gühlke, M.; Selve, S.; Kneipp, J. Magnetic Separation and SERS Observation of Analyte Molecules on Bifunctional Silver/Iron Oxide Composite Nanostructures. *J. Raman Spectrosc.* **2012**, *43*, 1204–1207.
31. Massart, R.; Cabuil, V. Effect of Some Parameters on the Formation of Colloidal Magnetite in Alkaline-Medium—Yield and Particle-Size Control. *J. Chem. Phys.* **1987**, *84*, 967–973.
32. van Ewijk, G. A.; Vroege, G. J.; Philipse, A. P. Convenient Preparation Methods for Magnetic Colloids. *J. Magn. Mater.* **1999**, *201*, 31–33.
33. Feng, J. J.; Gernert, U.; Hildebrandt, P.; Weidinger, I. M. Induced SER-Activity in Nanostructured Ag-Silica-Au Supports *via* Long-Range Plasmon Coupling. *Adv. Funct. Mater.* **2010**, *20*, 1954–1961.
34. Frickel, N.; Messing, R.; Gelbrich, T.; Schmidt, A. M. Functional Silanes as Surface Modifying Primers for the Preparation of Highly Stable and Well-Defined Magnetic Polymer Hybrids. *Langmuir* **2010**, *26*, 2839–2846.
35. Deng, Y.; Cai, Y.; Sun, Z.; Liu, J.; Liu, C.; Wei, J.; Li, W.; Wang, Y.; Zhao, D. Multifunctional Mesoporous Composite Microspheres with Well-Designed Nanostructure: A Highly Integrated Catalyst System. *J. Am. Chem. Soc.* **2010**, *132*, 8466–8473.
36. Sivanesan, A.; Ly, H. K.; Kozuch, J.; Sezer, M.; Kuhlmann, U.; Fischer, A.; Weidinger, I. M. Functionalized Ag Nanoparticles with Tunable Optical Properties for Selective Protein Analysis. *Chem. Commun.* **2011**, *47*, 3553–3555.
37. Link, S.; El-Sayed, M. A. Spectral Properties and Relaxation Dynamics of Surface Plasmon Electronic Oscillations in Gold and Silver Nanodots and Nanorods. *J. Phys. Chem. B* **1999**, *103*, 8410–8426.
38. Kelly, K. L.; Coronado, E.; Zhao, L. L.; Schatz, G. C. The Optical Properties of Metal Nanoparticles: The Influence of Size, Shape, and Dielectric Environment. *J. Phys. Chem. B* **2003**, *107*, 668–677.
39. Nie, S.; Emory, S. R. Probing Single Molecules and Single Nanoparticles by Surface-Enhanced Raman Scattering. *Science* **1997**, *275*, 1102–1106.
40. Lee, S. Y.; Hung, L.; Lang, G. S.; Cornett, J. E.; Mayergoyz, I. D.; Rabin, O. Dispersion in the SERS Enhancement with Silver Nanocube Dimers. *ACS Nano* **2010**, *4*, 5763–5772.
41. Halas, N. J.; Lal, S.; Chang, W. S.; Link, S.; Nordlander, P. Plasmons in Strongly Coupled Metallic Nanostructures. *Chem. Rev.* **2011**, *111*, 3913–3961.
42. Lee, P. C.; Meisel, D. Adsorption and Surface-Enhanced Raman of Dyes on Silver and Gold Sols. *J. Phys. Chem.* **1982**, *86*, 3391–3395.
43. Feng, M.; Tachikawa, H. Surface-Enhanced Resonance Raman Spectroscopic Characterization of the Protein Native Structure. *J. Am. Chem. Soc.* **2008**, *130*, 7443–7448.
44. Wanat, A.; Gdula-Argasinska, J.; Rutkowska-Zbik, D.; Witko, M.; Stochel, G.; van Eldik, R. Nitrite Binding to Metmyoglobin and Methemoglobin in Comparison to Nitric Oxide Binding. *J. Biol. Inorg. Chem.* **2002**, *7*, 165–176.
45. Jensen, F. B. Nitric Oxide Formation from Nitrite in Zebrafish. *J. Exp. Biol.* **2007**, *210*, 3387–3394.
46. Møller, J. K. S.; Skibsted, L. H. Mechanism of Nitrosylmyoglobin Autoxidation: Temperature and Oxygen Pressure Effects on the Two Consecutive Reactions. *Chem.—Eur. J.* **2004**, *10*, 2291–2300.
47. Nicoletti, F. P.; Howes, B. D.; Fittipaldi, M.; Fanali, G.; Fasano, M.; Ascenzi, P.; Smulevich, G. Ibuprofen Induces an Allosteric Conformational Transition in the Heme Complex of Human Serum Albumin with Significant Effects on Heme Ligation. *J. Am. Chem. Soc.* **2008**, *130*, 11677–11688.
48. Benko, B.; Yu, N. T. Resonance Raman Studies of Nitric Oxide Binding to Ferric and Ferrous Hemoproteins: Detection of Fe(III) −NO Stretching, Fe(III)—N—O Bending, and Fe(II)—N—O Bending Vibrations. *Proc. Natl. Acad. Sci. U.S.A.* **1983**, *80*, 7042–7046.
49. Guo, F.; Xu, X. X.; Sun, Z. Z.; Zhang, J. X.; Meng, Z. X.; Zheng, W.; Zhou, H. M.; Wang, B. L.; Zheng, Y. F. A Novel Amperometric Hydrogen Peroxide Biosensor Based on Electrospun Hb-Collagen Composite. *Colloids Surf., B* **2011**, *86*, 140–145.
50. Dou, Y.; Olson, J. S.; Wilkinson, A. J.; Ikeda-Saito, M. Mechanism of Hydrogen Cyanide Binding to Myoglobin. *Biochemistry* **1996**, *35*, 7107–7113.
51. Wazawa, T.; Matsuoka, A.; Tajima, G.; Sugawara, Y.; Nakamura, K.; Shikama, K. Hydrogen Peroxide Plays a Key Role in the Oxidation Reaction of Myoglobin by Molecular Oxygen. A Computer Simulation. *Biophys. J.* **1992**, *63*, 544–550.
52. Ascenzi, P.; di Masi, A.; Gullotta, F.; Mattu, M.; Ciaccio, C.; Coletta, M. Reductive Nitrosylation of Ferric Cyanide Horse Heart Myoglobin Is Limited by Cyanide Dissociation. *Biochem. Biophys. Res. Commun.* **2010**, *393*, 196–200.
53. http://water.epa.gov/drink/contaminants/basicinformation.
54. Olson, J. S.; Phillips, G. N. Myoglobin Discriminates between O_2, NO, and CO by Electrostatic Interactions with the Bound Ligand. *J. Biol. Inorg. Chem.* **1997**, *2*, 544–552.
55. Aime, S.; Fasano, M.; Paoletti, S.; Cutruzzola, F.; Desideri, A.; Bolognesi, M.; Rizzi, M.; Ascenzi, P. Structural Determinants of Fluoride and Formate Binding to Hemoglobin and Myoglobin: Crystallographic and ^{1}H-NMR Relaxometric Study. *Biophys. J.* **1996**, *70*, 482–488.
56. Nicoletti, F. P.; Comandini, A.; Bonamore, A.; Boechi, L.; Boubeta, F. M.; Feis, A.; Smulevich, G.; Boffi, A. Sulfide Binding Properties of Truncated Hemoglobins. *Biochemistry* **2010**, *49*, 2269–2278.
57. Yang, D.; Hu, J.; Fu, S. Controlled Synthesis of Magnetite-Silica Nanocomposites *via* a Seeded Sol−Gel Approach. *J. Phys. Chem. C* **2009**, *113*, 7646–7651.

58. Chen, L.; Hong, W.; Guo, Z.; Sa, Y.; Wang, X.; Jung, Y. M.; Zhao, B. Magnetic Assistance Highly Sensitive Protein Assay Based on Surface-Enhanced Resonance Raman Scattering. *J. Colloid Interface Sci.* **2012**, *368*, 282–286.
59. Jiao, T. F.; Zhou, J. A.; Zhou, J. X.; Gao, L. H.; Xing, Y. Y.; Li, X. H. Synthesis and Characterization of Chitosan-Based Schiff Base Compounds with Aromatic Substituent Groups. *Iran. Polym. J.* **2011**, *20*, 123–136.